Organic Electronics 13 (2012) 159–165

Contents lists available at SciVerse ScienceDirect

Organic Electronics

journal homepage: www.elsevier.com/locate/orgel

Letter

Efficiency enhancement of organic light emitting diode via surface energy transfer between exciton and surface plasmon

Arunandan Kumar [a,b], Ritu Srivastava [a,*], Priyanka Tyagi [a], D.S. Mehta [b], M.N. Kamalasanan [a]

[a] Center for Organic Electronics, National Physical Laboratory (Council of Scientific and Industrial Research), Dr. K.S. Krishnan Road, New Delhi 110012, India
[b] Instrument Design and Development Center, Indian Institute of Technology Delhi, New Delhi 110016, India

ARTICLE INFO

Article history:
Received 12 July 2011
Received in revised form 11 September 2011
Accepted 12 October 2011
Available online 1 November 2011

Keywords:
OLED
Surface plasmon
Surface energy transfer

ABSTRACT

Organic light emitting diodes (OLEDs) with surface plasmon (SP) enhanced emission have been fabricated. Gold nanoclusters (GNCs) deposited using thermal evaporation technique has been used for localization of surface plasmons. Size of GNCs and distance of GNCs from the emissive layer have been optimized using steady state and time resolved photoluminescence (PL) results. 3.2 Times enhancement in PL intensity and 2.8 times enhancement in electroluminescence intensity of OLED have been obtained when GNCs of size 9.3 nm has been introduced at a distance of 5 nm from emissive layer. Distance dependence of energy transfer efficiency between exciton and SPs was found to be of $1/R^4$ type, which is typically the dependence for dipole-surface energy transfer.

1. Introduction

The development of organic light emitting diodes (OLEDs) holds great promise for the production of highly efficient light sources [1]. They are fabricated using fluorescent and phosphorescent emissive materials [2,3]. Phosphorescent emissive materials are preferred over the fluorescent because in phosphorescent materials both triplet and singlet excitons can be exploited for emission while in case of fluorescent, only singlet excitons can emit [4,5]. The emission rate of a material is inversely proportional to the life time of excited state [6]. For high emission rate, the life time of excited state should be as small as possible. The excited state life time of phosphorescent materials is few μs in comparison to the few ns for fluorescent materials [7,8]. This is a disadvantage in case of phosphorescent materials.

Recently the coupling between excitons and surface plasmons (SPs) has been actively studied for radiative emission rate enhancement in semiconducting devices [9–12]. SPs are the collective oscillations of free electrons in a metal at the interfaces between the metal and dielectric [13–15]. They are propagating waves at metal/dielectric interface and coupling of light to SPs provide a major loss channel. However, the energy confined in the SP modes can be extracted as radiation through naturally formed surface imperfections such as nanostructures. The overlap of local electromagnetic field of the excitons in the emissive layer and SPs results in a coupling effect between them, due to which, effective energy transfer takes place between them creating an alternate channel for emission. Since the scattering of high momentum localized SPs (LSPs) is much faster than the decay of excitons, coupling results in the enhancement of radiation intensity. There are many reports regarding the use of localized SPs for the enhancement of internal quantum efficiency in inorganic LEDs [9,10]. The use of LSPs in OLEDs is limited to the photoluminescence only due to the difficulty in incorporating them inside the device structure at suitable place [11,12]. There are few reports available on the use of metallic nanoparticles for enhancing the efficiency of OLED [16–18], but the results are not significant. Fuziki et al. [16] have reported the use of gold nanoparticles to enhance the efficiency of OLED based on tris-(8-hydroxyquinolinato)aluminum (Alq_3) but the luminescence of

* Corresponding author.
E-mail address: ritu@mail.nplindia.org (R. Srivastava).

1566-1199/$ - see front matter © 2011 Elsevier B.V. All rights reserved.
doi:10.1016/j.orgel.2011.10.008

both the plasmon enhanced and reference OLED was poor ($\sim 10^{-3}$ Cd/m^2 at 12 V). Yang et al. [17] have used a cathode structure for plasmonic emission but their results on electroluminescence (EL) were not quite significant (e.g. they have got enhancement only for 2–5 V) and in the work of Choulis et al. [18], trapping due to gold nanoparticles is dominant.

In an exciton–SP system, there are two competitive processes; (i) radiation intensity enhancement due to LSPs and (ii) nonradiative losses due to metal. The efficiency of the interaction between LSPs and excitons exponentially decreases with increasing distance from the emissive layer to the metal surface [19]. At the same time, nonradiative quenching of exciton at metal surface occurs when the distance is very much smaller. Therefore for practical application, an appropriate distance between the emissive material and metal surface should be maintained to obtain radiation intensity enhancement. For the maximum coupling between exciton and SPs, the emission wavelength of excitons should match with the absorption wavelength of LSPs which depends upon the size of nanostructures [20,21]. Therefore, the size of nanostructures should be optimized for emission enhancement.

In this letter GNCs has been deposited by thermal evaporation and their effect on luminescence enhancement has been studied using steady state and time resolved photoluminescence. Size of GNCs and distance from the emissive layer has been optimized for maximum luminescence enhancement. GNCs have been inserted in phosphorescent OLED structure and the effect on the luminescence has been studied.

2. Experimental

Gold nanoclusters were fabricated by thermal evaporation at a base pressure of 4×10^{-6} Torr. OLEDs were fabricated on indium-tin-oxide (ITO) coated glass substrates having a sheet resistance of 20 Ω/□ and a thickness of 120 nm which were patterned and cleaned using deionised water, acetone, trichloroethylene and isopropyl alcohol sequentially for 20 min using an ultrasonic bath and dried in vacuum oven. Prior to organic film deposition ITO surface was treated with oxygen plasma for 5 min to increase ITO work function. Organic layers were deposited onto glass substrates under high vacuum (4×10^{-6} Torr) at a deposition rate of 0.4 Å/s. Thickness of the deposited layers were measured in situ by a quartz crystal thickness monitor. The device structure was ITO (120 nm)/α-NPD (30 nm)/5% Ir(ppy)$_3$ doped CBP (35 nm)/BCP (6 nm)/Alq$_3$ (28 nm)/LiF (1 nm)/Al (150 nm). Tris-(8-hydroxyquinoline)aluminum (Alq$_3$) (Sigma Aldrich) and *N*,*N*′-Di-[(1-naphthalenyl)-*N*,*N*′-diphenyl]-(1-1′-biphenyl)-4,4′-diamine (α-NPD) (Sigma Aldrich) were used as the electron and hole transporting layers. 2,9-dimethyl-4,7-diphenyl-1,10-phenanthrolene (BCP) (Sigma Aldrich) which has a high ionization potential (6.5 eV) has been used as hole blocking layer and lithium fluoride (LiF)/aluminum (Al) and ITO has been used as cathode and anode, respectively. The size of each pixel was 5 mm × 5 mm. UV–Vis absorption spectrum was recorded using a Shimadzu UV–Vis spectrophotometer model No. UV-2401 PV. Steady state and time resolved photoluminescence spectra were studied using a Fluorolog (Jobin Yvon – Horiba, model-3-11) spectrofluorometer at room temperature. Using high pressure xenon lamp for steady state and 370 nm wavelength LED having pulse time of 1 ns for time resolved. EL spectrum has been measured with a high resolution spectrometer (Ocean optics HR-2000 CG UV-NIR). The current density–voltage–luminescence (*J*–*V*–*L*) characteristics have been measured with a luminance meter (LMT-1009) interfaced with a keithley 2400 programmable current–voltage digital source meter. All the measurements were carried out at room temperature under ambient conditions.

3. Results and discussion

Fig. 1(a) shows the AFM image of GNCs thermally evaporated on glass substrates with deposition rate 0.1 nm/s. The image shows a distribution of particle size. The average size of these GNCs has been calculated from the AFM results for different deposition rates and is shown in Fig. 1(b) which shows an increase in particle size with the increase in deposition rate. Since the size of GNCs is very important for the study of LSP resonance (LSPR), the results have been repeated three times and the variation in size were found to be within ±5%. The average size of the GNCs was found to vary from 5 to 14 nm with the variation of deposition rate from 0.05 to 0.2 nm/s.

The next important parameter for the study of LSPR is the absorption spectrum of GNCs. Fig. 2(a) shows the absorption spectrum of the GNC samples of different sizes. The wavelength corresponding to maximum absorption (LSPR wavelength) has been obtained and drawn in Fig. 2(b) as a function of GNC size. This wavelength is found to increase with the increase in GNC size. This type of wavelength shift with particle size is commonly observed in metallic nanoparticles [20,21]. Coupling between the exciton and surface plasmons has been found to affect (increase/decrease) the spontaneous emission rate from dipoles and is a near field effect. Numerical modeling indicates that the near field due to metallic nanoparticles decays very fast with distance and becomes negligible at distances comparable to the particle size [22]. Coupling of dipole near field with NC near field affects the decay time of excited states of emitting dipole and is responsible for

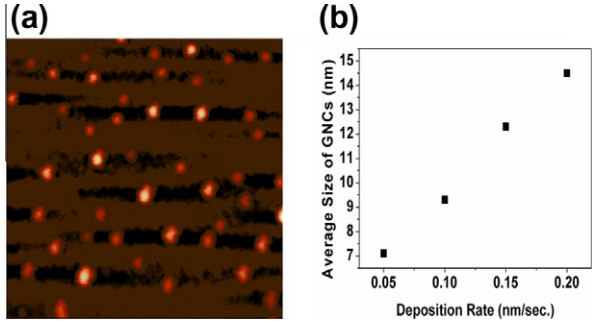

Fig. 1. (a) AFM image of GNCs deposited with deposition rate of 0.1 nm/s, (b) Variation of average particle size with deposition rate.

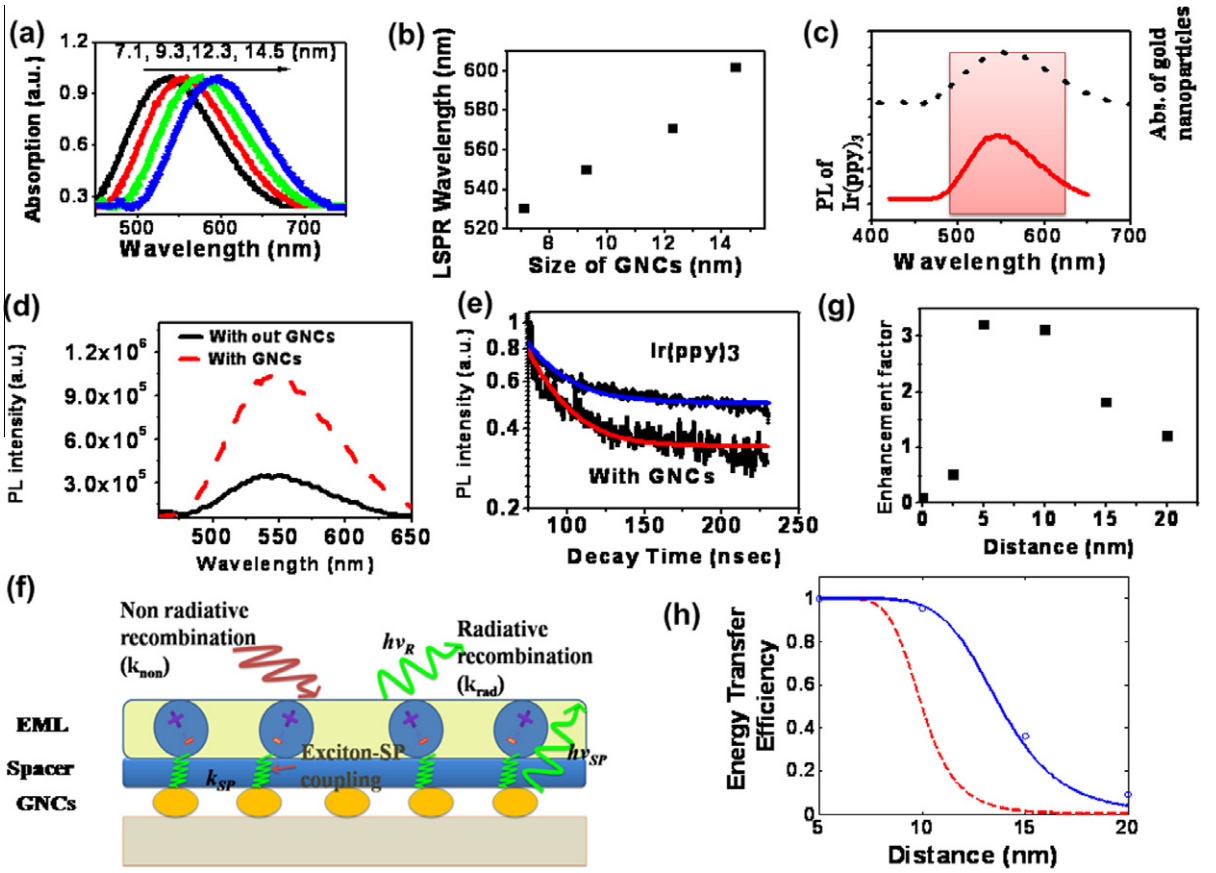

Fig. 2. (a) Absorption spectrum of GNCs with different deposition rates, (b) variation in LSPR wavelength with size of GNCs, (c) overlap between absorption spectrum of GNCs and emission spectrum of $Ir(ppy)_3$, (d) PL intensity of $Ir(ppy)_3$ without GNCs and after incorporating GNCs, (e) time resolved PL spectrum of samples with and without GNCs, (f) schematic diagram showing typical mechanism for exciton–SP coupling, (g) enhancement ratio for different spacing between emissive layer and GNCs, (f) PL intensity for samples with and without GNCs, (h) experimental and theoretical energy transfer efficiency for exciton–SP system as a function of distance between emissive layer and GNCs (black squares are experimental points, solid line is theoretical energy transfer efficiency for SET mechanism and dashed line is for FRET mechanism).

the enhancement as well as decrease in emission rate [19]. The enhancement occurs when the absorption spectrum of SPs at metal surfaces matches with the emission spectrum of dipoles. Dipolar strength of emitting dipole is an important parameter in this coupling. Dipolar strength of triplet emitter is smaller than that of the singlet emitter. The spatial density of photonic states does not depend on the oscillator strength due to which the emission rate enhancement for singlet and triplet emitter occurs at the same length scale. Besides the emission rate acceleration, interactions with the metal surface introduce nonradiative losses due to the Forster energy transfer from dipoles to the metal. The rate of this energy transfer process scales as f/R^m, where f is the oscillator strength of the emitting dipole, R is the distance between the emitter and metal surface and m depends on geometrical factors [19]. Since triplet emitters have smaller oscillator strength in comparison to singlet emitters, the nonradiative losses occur at a very small length scale of the order of 2 nm for triplet emitters compared to the 20 nm for singlet emitters [19]. This causes the nonradiative losses for singlet emitters to be much larger than that for triplet emitters. Therefore, a thin spacer can be placed between the emitter and metal surface and by changing its thickness, distance between the emitter and metal surface can be tuned to control the nonradiative losses and to achieve emission rate enhancement due to surface plasmon resonance.

In the present study, we have selected a triplet emitter $Ir(ppy)_3$ as an emitting material, GNCs for coupling of triplet states with the surface plasmons and LiF as a spacer to control the distance between the GNCs and $Ir(ppy)_3$. Since the maximum coupling between the emitter and SPs at GNC surface will occur when the emission spectrum of emitter matches with the absorption spectrum of SPs at metal surface, we have recorded the emission spectrum of $Ir(ppy)_3$ and compared it with the absorption spectrum of GNCs of different sizes. Fig. 2(c) shows the absorption spectrum of GNCs of size 9.3 nm and emission spectrum of $Ir(ppy)_3$. The overlap between the two spectrums is found to be 94%. The excellent overlap between the two spectrum suggests them to be used for SP–exciton coupling. The samples to study the effect of SPs on photoluminescence have been fabricated on glass

substrates on which GNCs of size 9 nm have been deposited using thermal evaporation. Over the top of GNCs a spacing layer of LiF (5 nm) and emissive layer (50 nm) have been evaporated. For emissive layer, $Ir(ppy)_3$ has been used. For the photoluminescence studies, the excitation wavelength has been fixed at 370 nm. This excitation wavelength is very much far from the absorption wavelength of SPs on GNC surface (~540 nm), which avoids the possibilities of simultaneous excitation of SPs and emitter. For pure $Ir(ppy)_3$, the intensity obtained was found to be quite low due to luminescence quenching as a result of triplet–triplet annihilation. Due to this $Ir(ppy)_3$ has been dispersed in CBP in small concentration (5%) by co-evaporation of $Ir(ppy)_3$ and CBP which shows strong PL. Fig. 2(d) shows the PL spectrum of 5% $Ir(ppy)_3$ doped CBP with and without GNCs. It has been seen that the peak PL intensity has been enhanced by 3.2 times for the sample with GNCs compared to the samples without GNCs. Since the excited state life time of emitter decreases with the increase in coupling between the triplet exciton and surface plasmon, we have made a detailed study on the excited state life time of the triplet emitter without and with GNCs at different distances from emitter. Fig. 2(e) shows the time resolved PL intensity for the samples with and without the GNCs. The decay profile includes more than one decay components. $Ir(ppy)_3$ have more than one MLCT states which have different decay times. Therefore, more than one components have been observed in the PL decay [23]. The life time of fast component of excited state has been calculated and the values were 0.1 and 0.35 μs for samples with and without the GNCs. Since the spontaneous emission rate is proportional to the spontaneous emission coefficients and is inversely proportional to the excited state life time, hence spontaneous emission rate is expected to increase with the decrease in the excited state life time. Similar changes in radiative decay life time has been observed by Neal et al. [24].

The possible mechanism can be understood using the schematic diagram given in Fig. 2(f). First, excitons are generated in the emissive layer by exciting it with its excitation wavelength. Inside the emissive layer, the excitons can decay either radiatively (k_{rad}) or nonradiatively (k_{non}). The quantum efficiency of radiative decay is given by $\eta_{int} = k_{rad}/(k_{rad} + k_{non})$. When a metal layer is grown very close to the emissive layer, and the emission wavelength of emitting material is close to the LSPR wavelength, then energy transfer will occur between exciton and SPs. The rate of energy transfer is given by k_{SP}. SP modes have very large density of states which creates a very high electromagnetic field. PL decay rates increases because the values of k_{SP} are quite high. In general, coupling to SP modes decrease the efficiency because these SP waves are evanescent. These SP modes can be scattered and made radiative by using metallic nanostructures. In our experiments the roughness of GNCs makes the SPs to decay radiatively [25].

The distance between the emitter and GNCs is an important parameter in the study of exciton–SP coupling. In our samples, the distance has been tuned by changing the thickness of spacing layer (LiF). Fig. 2(g) shows the enhancement factor with different thickness of LiF. It can be seen that for thickness <5 nm, the emission intensity has reduced, which may be due to the nonradiative decay at metal surface by Forster type energy transfer from exciton to metal surface. As the distance is increased to 5 nm, nonradiative decay has decreased and the emission intensity has increased by 3.2 times. As the thickness of LiF increases further to 10 nm, exciton–SP coupling weakens and enhancement in emission intensity starts decreasing and becomes 2.8. With further increase in the thickness of LiF (>10 nm), the enhancement rate approaches to unity. These results suggest a strong distance dependent energy transfer efficiency between exciton and SP modes. We have also calculated the radiative and nonradiative rate constants using the radiative decay life time and PL efficiency data. Fig. 3(a) shows the plots of k_{rad} and k_{non} as a function of distance. It can be seen that k_{rad} and k_{non} varies with distance. k_{rad} first increases with the distance up to 5 nm and then starts decreasing with increase in distance. The energy transfer efficiency $E(R) = 1 - I(R)/I_\infty$ has been calculated for different separation distances, where I_∞ is the PL intensity for the samples without GNCs and $I(R)$ is the PL intensity when GNCs are placed at a distance R from the emissive layer. Fig. 2(h) shows the energy transfer efficiency with the separation distance. In general the quantum efficiency of energy transfer can be written as [22]:

$$E(r) = \frac{1}{1 + \left(\frac{r}{r_0}\right)^m}. \quad (1)$$

In the case of dipole–dipole energy transfer $m = 6$ and $r_0 = R_0$ (Forster radius), whereas for dipole–surface energy transfer $m = 4$ and $r_0 = d_0$, where d_0 is given by Persson and Lang's equation [26]:

$$d_0 = \left(0.525 \frac{c^3 \Phi_D}{\omega^2 \omega_F k_F}\right)^{1/4}. \quad (2)$$

And is a function of donor quantum efficiency (Φ_D), the frequency of the donor electronic transition (ω); Fermi frequency (ω_F), and Fermi wave vector (k_F) of the metal. The theoretical energy transfer efficiency has been calculated from Eq. (1) for a pure dipole–dipole (FRET) and dipole–surface energy transfer (SET) processes and plotted in Fig. 2(g). The Forster radius calculated using Forster equation [27] is 5.2 nm, while the SET radius (d_0), calculated using Eq. (2) is 8.8 nm. The parameters used to calculate d_0 were $\Phi_D = 0.65$, $\omega = 3.5 \times 10^{15}\ s^{-1}$, $\omega_F = 8.4 \times 10^{15}\ s^{-1}$, and $k_F = 1.2 \times 10$ $8\ cm^{-1}$, which are bulk Au and emissive layer constants, while R_0 is calculated using spectral overlap of GNCs absorbance and emissive layer PL spectrum. Comparison of the theoretical and experimental energy transfer efficiencies indicates poor agreement with a Forster mechanism and an excellent agreement with dipole–surface energy transfer mechanism.

We have also measured the changes in PL intensity for the GNCs having different sizes. Fig. 3(b) shows the enhancement factor against the separation distance for the GNCs having different sizes. It can be seen that as the size of GNCs change the enhancement factor decreases. This may be ascribed due to the shift in LSPR wavelength with the change in size and the shift is causing the coupling between the exciton and SPs to be weak for the GNCs having sizes other than 9.3 nm. The results were found

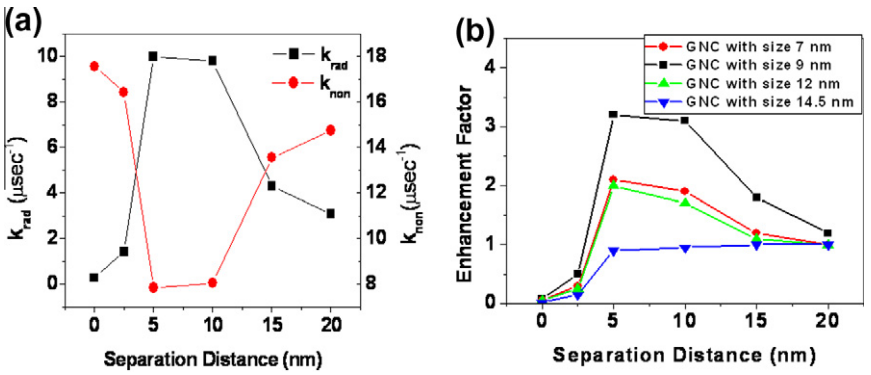

Fig. 3. (a) Radiative and nonradiative decay rate constants as a function of separation distance, (b) PL enhancement factor for the GNCs with different sizes.

consistent with the previous reports on exciton–SP coupling in different inorganic-metal nanostructure systems [20,21].

The GNCs deposited using vacuum evaporation technique has been used to enhance the emission efficiencies of OLEDs. Since the insertion of the GNCs in OLED structure changes the current flowing through the diode, their insertion in diode structure requires more optimization in comparison to the PL samples. The efficiency of an OLED can only be compared if the current density of the device remains same after the incorporation of GNCs. Therefore, the GNC density has been adjusted in such a way that it does not seriously affect the current flowing through the device. This has been done by optimizing the cluster density by controlling the cluster deposition rate. Samples with device structure shown in Fig. 4(a) have been fabricated having different duration of gold deposition to realize different cluster density and the deposition rate was kept fixed at 0.1 nm/s so as to have the size of GNCs to be 9.3 nm. The used materials for fabricating the OLED are given in experimental section. HTL, EML, HBL, ETL are acronyms for hole transport layer, emissive layer, hole blocking layer, electron transport layer, respectively. Duration of deposition has been varied and total four samples have been prepared for the duration of 10, 20, 35, 50 s. For reference, a device without GNCs has also been fabricated. Fig. 4(b) shows the current density–voltage (*J–V*) characteristics for the samples with and without GNCs. It can be seen that when the duration of deposition is less than 2 min, the *J–V* characteristics are almost identical to the reference device and as the duration of deposition increases, current density starts to decrease. The reason behind the decrease in current density may be the trapping of charges in GNCs. Before proceeding further to use this duration of deposition, it is essential to check that the size of GNCs has not been affected. Fig. 4(c) shows the AFM image of GNCs deposited for 20 s. duration. This sample contains all the layers as used for the OLED fabrication. The particle size of GNCs was calculated and found to be 9.3 nm. Absorption spectrum has also been measured and found to be unchanged from Fig. 2(a).

After optimizing the duration of deposition, the distance between the emitting layer and GNCs has been optimized. We have prepared four samples with device structure shown in Fig. 5(a–d). In first device, GNCs are just deposited on emissive layer, in second, GNCs were deposited in between HBL and ETL, in third, GNCs were deposited inside the ETL at a distance 5 nm from HBL and in fourth GNCs were 10 nm away from HBL inside the ETL. In this way the distance of GNCs from EML has been tuned from 0 to 15 nm in step of 5 nm. A reference device has also been fabricated in which the GNCs were not deposited. All of the SP devices have the same *J–V* characteristics as the reference device. Fig. 5(e–h) shows the current density–luminescence (*J–L*) characteristics for these devices. *J–L* characteristics of the reference device are also shown

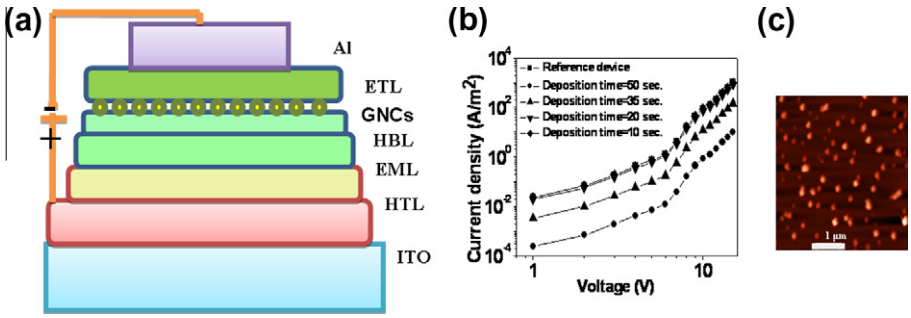

Fig. 4. (a) Device structure of GNCs incorporated OLED for the study of current density, (b) current density–voltage characteristics for the OLEDs for different deposition durations of GNCs, (c) AFM image of GNCs deposited on top of HBL for 2 min at a rate of 1 nm/s.

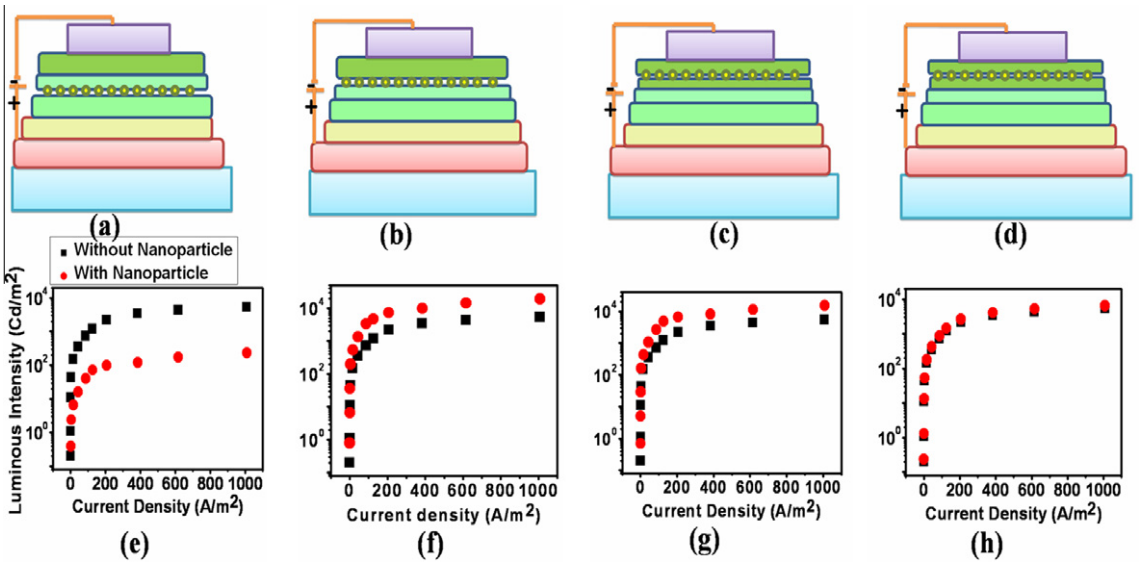

Fig. 5. Current density–luminescence characteristics for OLEDs with GNCs inserted at different places (a and e) device structure and *L–J* characteristics for the device in which GNCs are inserted at EML/HBL interface, (b and f) device structure and *L–J* characteristics for the device in which GNCs are inserted at HBL/ETL interface (distance of GNCs from EML is 5 nm), (c and g) device structure and *L–J* characteristics for the device in which GNCs are inserted inside ETL at a distance of 5 nm from the HBL/ETL interface (distance of GNCs from EML is 10 nm), (d and h) device structure and *L–J* characteristics for the device in which GNCs are inserted inside ETL at a distance of 10 nm from the HBL/ETL interface (distance of GNCs from EML is 15 nm). The layers used in the device structure are glass, ITO, HTL, EML, HBL, ETL, Al from bottom.

in all of the curves for comparison. It can be seen that for the first device, the luminescence is quite low in comparison to the reference device. The reason may be the nonradiative decay occurring at metal surface as also observed in the case of PL results. For device 2 and 3, the luminescence has been enhanced in comparison to the reference device. For device 2, the enhancement is about 2.8 times and for device 3, the enhancement is about 2.2 times. But, further increase in the distance between the emissive layer and GNCs did not increase the luminescence much as can be seen in Fig. 5(h), which suggests that the distance is too large for the exciton–SP coupling. Table 1 shows the comparison of the luminance, current efficiency and external quantum efficiency of devices 1, 2, 3, 4 and the reference device.

In conclusion GNCs have been deposited using thermal evaporation technique. Size of GNCs has been tuned by changing the deposition rate of gold. LSPR wavelength has been found to be dependent on GNC sizes and a red shift in LSPR wavelength has been observed with the increase in particle size. Exciton–SP coupling has been studied using a device structure GNC/LiF/5% $Ir(ppy)_3$ doped CBP. Thickness of LiF has been changed to study the distance dependence of exciton–SP coupling. Nonradiative quenching of excitons was found dominant for less than 5 nm distance between emissive material and GNCs. When the distance was increased further, the radiative rate enhancement started to occur. After a certain distance, radiative rate did not increase. Energy transfer efficiency from exciton to SPs has been calculated for each distance. It scaled as R^{-4} with distance, which is the typical dependence in the case of dipole–surface energy transfer with excitons behaving like dipole and GNCs as surface. OLEDs have been fabricated after incorporating GNCs to see the effect of SPs on OLED efficiency. First, the GNC density has been optimized to reduce the trapping effects on current due to GNCs. The distance of GNC has been varied from the emissive layer and the effect on luminous intensity has been observed. Luminous intensity reduced quite significantly, when the GNCs were just adjacent to the emissive layer and it has increased about 2.8 times for distance of 5 nm. With further increase of distance to 10 nm has decreased the enhancement of intensity to 2.2 times. Luminous intensity remained unaffected for larger distances between emissive layer and GNCs.

Table 1
Luminous, current and external quantum efficiency of reference device and device with GNCs.

	Luminance (in cd/m^2 at 12 V)	Current efficiency (in cd/A at12 V)	External quantum efficiency (in % at 12 V)
Reference device	2210	10.7	2.1
Device 1	98	0.48	0.01
Device 2	7260	35.2	6.9
Device 3	6530	31.6	6.2
Device 4	2650	12.8	2.5

Acknowledgement

Authors are thankful to Director, National Physical Laboratory, New Delhi for continuous encouragement. The Authors also gratefully recognize the financial support from the Department of Science and Technology (DST)

and Council of Scientific and Industrial Research (CSIR) New Delhi, India for the projects – NWP-25.

Appendix A. Supplementary data

Supplementary data associated with this article can be found, in the online version, at doi:10.1016/j.orgel.2011.10.008.

References

[1] J. Kido, M. Kimura, K. Nagai, Science 267 (1995) 1332–1334.
[2] C.W. Tang, S.A. Vanslyke, Appl. Phys. Lett. 51 (1987) 913.
[3] Y. Sun, N.C. Giebink, H. Kanno, M. Biwu, M.E. Thompson, S.R. Forrest, Nature 440 (2006) 908.
[4] S. Reineke, F. Lindner, G. Schwartz, N. Seidler, K. Walzer, B. Lussem, K. Leo, Nature 459 (2009) 234.
[5] Y. Sun, S.R. Forrest, Appl. Phys. Lett. 91 (2007) 263503.
[6] W.T. Silfvast, Laser Principle and Application, Cambridge University Press, 2004.
[7] N.C. Giebink, S.R. Forrest, Phys. Rev. B 77 (2008) 235215.
[8] A.K. Bansal, A. Penzkofer, W. Holzer, T. Tsuboi, Ukr. J. Phys. 52 (2007) 353.
[9] K. Okamoto, N. Isamu, A. Shvartser, Y. Narukawa, T. Mukai, A. Scherer, Nat. Mater. 3 (2004) 601.
[10] M.K. Kwon, J.-Y. Kim, B.-H. Kim, I.-K. Park, C.-Y. Cho, C.C. Byeon, S.-J. Park, Adv. Mater. 20 (2008) 253.
[11] M.C. Tam, H. Su, K.S. Wong, X. Zhu, H.S. Kwok, Appl. Phys. Lett. 95 (2009) 051503.
[12] K.H. Cho, S.I. Ahn, S.M. Lee, C.S. Choi, K.C. Choi, Appl. Phys. Lett. 97 (2010) 193306.
[13] K. Munechika, Y. Chen, A.F. Tillack, A.P. Kulkarni, I.J.L. Plata, A.M. Munro, D.S. Ginger, Nano Lett. 10 (2010) 2598.
[14] P.A. Hobson, J.A.E. Wasey, I. Sage, W.L. Barnes, IEEE J. Sel. Top. Quantum Electron. 8 (2002) 378.
[15] J.M. Pitarke, V.M. Silkin, E.V. Chulkov, P.M. Echenique, Rep. Prog. Phys. 70 (2007) 1–87.
[16] A. Fuziki, Uemura, N. Zettsu, M.A. Kasaya, A. Saito, Y. Kuwahara, Appl. Phys. Lett. 96 (2010) 043307.
[17] K.Y. Yang, K.C. Choi, C.W. Ahn, Appl. Phys. Lett. 94 (2009) 173301.
[18] S.A. Choulis, M.K. Mathai, V.-E. Choong, Appl. Phys. Lett. 88 (2006) 213506.
[19] J.C. Ostrowski, A. Mikhailovsky, A. Bussian, M.A. Summers, S.K. Buratto, G.C. Bazan, Adv. Funct. Mater. 16 (2006) 1221.
[20] P. Viste, J. Plain, R. Jaffiol, A. Vial, P.M. Adam, P. Royer, ACS Nano 4 (2010) 759.
[21] S. Link, M.A. El-Sayed, J. Phys. Chem. B 103 (1999) 4212.
[22] C.S. Yun, A. Javier, T. Jennings, M. Fisher, S. Hira, S. Peterson, B. Hopkins, N.O. Reich, G.F. Strause, J. Am. Chem. Soc. 127 (2005) 3115.
[23] W.J. Finkenzeller, H. Yersin, Chem. Phys. Lett. 377 (2003) 299.
[24] T.D. Neal, K. Okamoto, A. Scherer, M.S. Liu, A.K.-Y. Jen, Appl. Phys. Lett. 89 (2006) 221106.
[25] K. Okamoto, I. Niki, A. Scherer, Y. Narukawa, T. Mukai, Y. Kawakami, Appl. Phys. Lett. 87 (2005) 071102.
[26] B. Persson, N. Lang, Phys. Rev. B 26 (1982) 5409.
[27] T. Forster, Discuss. Faraday Soc. 27 (1954).